Available online at www.sciencedirect.com
ScienceDirect
Advances in Space Research 46 (2010) 642–650
ADVANCES IN SPACE RESEARCH (a COSPAR publication)
www.elsevier.com/locate/asr

High vertical resolution water vapour profiles in the upper troposphere and lower stratosphere retrieved from MAESTRO solar occultation spectra

C.E. Sioris [a,*], J. Zou [b], C.T. McElroy [a], C.A. McLinden [a], H. Vömel [c]

[a] Environment Canada, 4905 Dufferin St., Toronto, ON, Canada M3H 5T4
[b] University of Toronto, 60 St. George St., Toronto, ON, Canada M5S 1A7
[c] Deutscher Wetterdienst, Meteorologisches Observatorium Lindenberg, Richard Assmann Observatorium, Am Observatorium 12, 15848 Tauche/Lindenberg, Germany

Received 7 July 2009; received in revised form 30 March 2010; accepted 30 April 2010

Abstract

An algorithm has been developed that retrieves water vapour profiles in the upper troposphere and lower stratosphere from optical depth spectra obtained by the Measurements of Aerosol Extinction in the Stratosphere and Troposphere Retrieved by Occultation (MAESTRO) instrument onboard the SCISAT satellite as part of the Atmospheric Chemistry Experiment (ACE) mission. The retrieval relies on ro-vibrational absorption of solar radiation by water vapour in the 926–970 nm range. During the iterative inversion process, the optical depth spectra are simulated at the spectral resolution and sampling frequency of MAESTRO using the correlated-*k* approximation. The Chahine inversion updates the water vapour volume mixing ratio (VMR), adjusting all retrieval layers simultaneously, to match the observed differential optical depth due to absorption by water vapour and ozone at each tangent height. This approach accounts for significant line saturation effects. Profiles are typically obtained from ~22 km down to the cloud tops or to 5 km, with relative precision as small as 3% in the troposphere. In the lower stratosphere, the precision on water vapour VMR is ~1.3 μmol/mol in an individual retrieval layer (~1 km thick). The spectral capability of MAESTRO allows for the clear separation of extinction due to water vapour and aerosol, and for the fitting quality to be quantified and used to determine an altitude-dependent convergence criterion for the retrieval. In the middle troposphere, interhemispheric differences in water vapour VMR are driven by oceanic evaporation whereas in the upper troposphere, deep convection dominates and a strong seasonal cycle is observed at high latitudes.

Keywords: Remote sensing; Near-infrared; Solar occultation

1. Introduction

Water vapour ($H_2O(v)$) is the most important atmospheric gas contributing to the radiation budget in the troposphere. Water vapour vertical profile information is valuable for understanding the distribution of clouds and their optical depth. In the stratosphere, water vapour appears to have an important feedback on the depletion of ozone, as increased $H_2O(v)$ also translates to thicker polar stratospheric clouds and increased OH concentration which leads to an increased ozone destruction rate (*e.g.* Kirk-Davidoff et al., 1999).

Space-based remote sounding of $H_2O(v)$ in the upper troposphere and lower stratosphere (UT/LS) is currently being performed by Microwave Limb Sounder onboard the Aura satellite (Aura-MLS), and was done previously on UARS (Upper Atmosphere Research Satellite). Aura-MLS can measure down to 316 mbar (*e.g.* Su et al., 2006) or approximately 9 km. The nadir-viewing AIRS has a vertical resolution of 2 km in the troposphere, but its ~10 μmol/mol lower detection limit (Gettelman et al.,

* Corresponding author. Tel.: +1 (416) 739 4929; fax: +1 (416) 739 4281.
E-mail address: csioris@cfa.harvard.edu (C.E. Sioris).

0273-1177/$36.00
doi:10.1016/j.asr.2010.04.040

2004) makes water vapour at the tropopause and in the stratosphere difficult to detect. The mid-infrared (IR) limb-viewing MIPAS measures water vapour profiles at coarse vertical resolution ($\geqslant$4.5 km) (Milz et al., 2005). Water vapour profiles have also been observed by recent mid-IR solar occultation instruments such as ILAS, ILAS-2, and HALOE and are currently measured by the ACE Fourier Transform Spectrometer (FTS) on SCISAT (Nassar et al., 2005).

From the literature, it would appear that only the near-IR-observing occultation instruments such as POAM III and SAGE II have provided published profiles of H_2O(v) at 1 km resolution in the UT/LS from space, but because of the discrete-channel design of these instruments, they had difficulty in discriminating between aerosol and water vapour extinction and, consequently, the validity of SAGE II profiles is limited to conditions with low aerosol extinction (Taha et al., 2004). For POAM III, residual aerosol errors for water vapour at 10 km are ~100% for 1018 nm extinction of 0.001 km^{-1}, which is typical for air just above the mid-latitude tropopause (Lumpe et al., 2002). For MAESTRO (Measurements of Aerosol Extinction in the Stratosphere and Troposphere Retrieved by Occultation) (McElroy et al., 2007) onboard SCISAT, with its ~2 nm spectral resolution at 940 nm and its spectral range of 509–1013 nm in the 'VIS' channel, the separation of aerosol and water vapour extinction is straightforward. Much like MAESTRO, SAGE III can also be expected to be able to discriminate between broadband aerosol extinction and discrete water vapour absorption. At present, SAGE III water vapour data has not been published and the instrument is no longer in operation. Hence, the water vapour data from MAESTRO, presented here, is a unique product with high value for the UT/LS community given the importance of this constituent to climate and chemistry and the need for high vertical resolution profiles for the study of various atmospheric phenomena, such as microphysical processes on thin clouds in the tropopause transition layer and upper troposphere. Furthermore, and in contrast to SAGE III which flew onboard the Meteor-3 M satellite, the SCISAT orbit provides periodic coverage of all latitudes, so that studies of regions like the TTL and the austral and boreal polar vortex are all possible. The SCISAT satellite was launched in August 2003 and MAESTRO spectra have been recorded from February 2004 to the present.

2. Method

The MAESTRO instrument and the calibration procedure, as well as the viewing geometry are described by McElroy et al. (2007). Briefly, solar occultation measurement opportunities occur when, from the vantage point of the satellite, the sun is slightly above the horizon, and is rising or setting. At these moments, the sun's rays are tangential to the Earth's atmosphere at the so-called tangent point. The altitude of this point is referred to as the tangent height. As the sun rises or sets, the tangent point moves quasi-vertically through the atmosphere, allowing for observations at a series of tangent heights. Spectra of transmitted solar irradiance including absorption features due to ozone and water vapour are measured by a grating spectrometer covering the 509–1013 nm range with a 1024 element Reticon photodiode array for light detection. A second grating spectrometer covers shorter wavelengths from 285 to 545 nm. MAESTRO's instantaneous field of view (FOV) translates to ~1.2 km (vertical) by ~25 km (horizontal).

The water vapour retrieval algorithm was briefly described previously (Carleer et al., 2008). The retrieval method consists of matching observed differential optical depth, averaged over the water vapour absorption window (926.0–969.7 nm) with simulated optical depth spectra, averaged over the same wavelength range. The solar spectrum is modeled at high resolution and integrated over the instrument line-shape function to match the observed optical depths. In contrast to methods which simulate the measured water vapour absorption by including a water vapour cross section in the spectral fitting of the optical depth spectra (*e.g.* McElroy et al., 2007), this approach allows saturation effects to be taken into account, which are significant, particularly in the troposphere. The optical depth baseline, resulting mostly from aerosol extinction, is assumed to be linear between the end points of this fitting window and the removal of this baseline yields differential absorption optical depth spectra. The fitting window has differential spectral structure due mostly to absorption by water vapour, but also by ozone through the 2-0 band of the Wulf system (*e.g.* El Helou et al. (2005), see Fig. 1). Extinction due to aerosols and Rayleigh scattering is expected to be approximately linear given the limited spectral range of the fitting window and the relatively small values of background extinction under the clear-sky conditions existing when measurements are possible.

The motivation behind using a wavelength-averaged observable is that the strength of a vibrational absorption band is independent of temperature (Bernath, 1995) for temperatures sufficiently low that the sum of the line intensities of transitions arising from vibrationally-excited initial states is relatively insignificant. This is the case in the water vapour absorption window for the range of temperatures occurring in the upper troposphere and lower stratosphere. On the other hand, fitting optical depth spectra is much more dependent on the knowledge of the atmospheric temperature profile.

The upper altitude limit of the retrieval is variable and corresponds to the tangent height (TH) for which the spectrally-averaged differential optical depth is >0.01005 (lower detection limit: LDL, derived empirically), and is so for all underlying THs. The typical upper limit of the retrieval is ~22 km. The lower altitude limit of the retrieval is generally determined by clouds for both sunsets and sunrises. When a cloud blocks the view of the sun, there is a loss of pointing reliability as the satellite's sun-tracking mirror

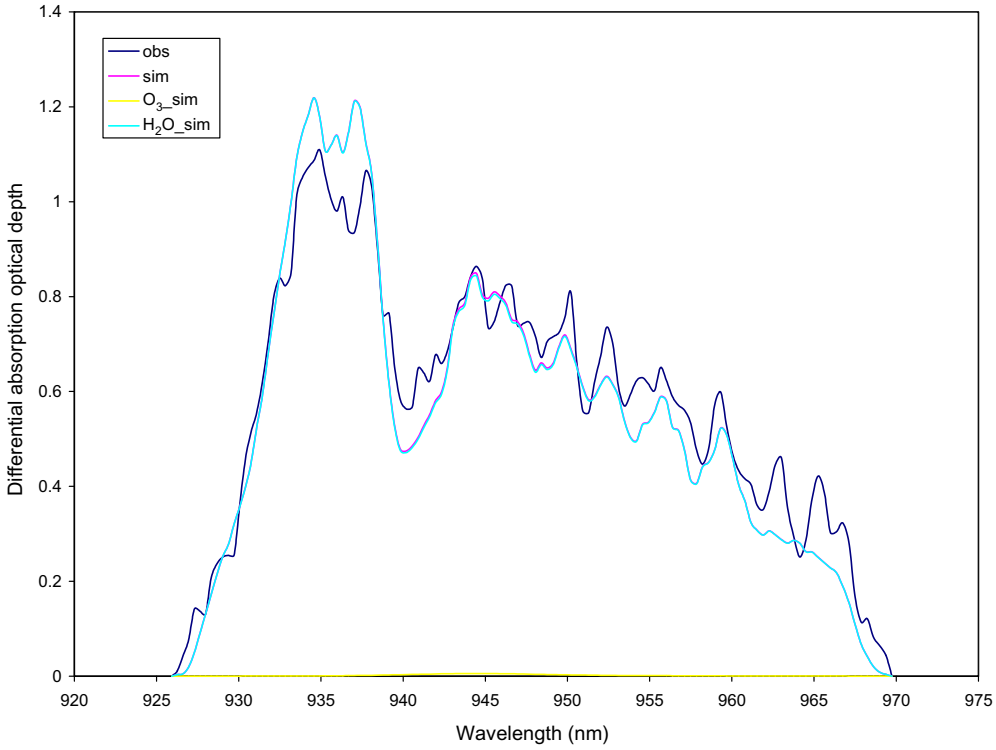

Fig. 1. Observed ('obs') and simulated ('sim') differential absorption optical depth spectra for TH = 9.56 km on July 29, 2005. 'O3_sim' and 'H2O_sim' are the simulated differential optical depth due to absorption by ozone and water vapour, respectively. The observed wavelength-averaged value is 0.6091.

effectively fails, and a decrease in the quality of the optical spectra is readily detectable. Thus, the data, to some extent, are somewhat biased toward clear-sky conditions. Spectra measured with optically thin and/or broken clouds in the field-of-view may still be included, but the lower limit of the retrieval is always $\geqslant 5.0$ km.

Other quality control steps applied to the optical depth spectra (Level 1 data) include the removal of tangent heights from the retrieval with negative optical depths or optical depths >7.63 (derived empirically) at any of the 96 pixels in the water vapour fitting window. After these quality control steps, the inversion begins, provided that all usable adjacent tangent heights are within 5 km of each other.

The inversion operates on the tangent height grid of the measurements. The vertical sampling varies with the angle between the orbit plane and the sun-to-sensor vector, namely the beta angle, but is better than 1 km typically in the UT/LS and ~1 km in the middle stratosphere. Based on the latitude and season of the measurement, the model atmosphere (pressure, temperature) and the first guess water vapour profile are selected from model atmospheres 1–5 in MODTRAN4, revision 1 (Berk et al., 1999). Optical depth spectra are simulated with MODTRAN4 at the spectral resolution (20 cm^{-1}) and sampling (4 cm^{-1}) of MAESTRO to mimic instrumental effects. At 940 nm, the spectral sampling and resolution are 0.4 and 1.8 nm, respectively. The spectral resolution in the water vapour spectral window was determined empirically by fitting in-flight observations with simulations at different spectral resolution since the wavelength dispersion was not known with sufficient accuracy before launch. The spectral sampling depends on the wavelength to pixel mapping. The pre-launch wavelength calibration was also not sufficiently accurate, based on in-flight observations of Fraunhofer line positions. Fig. 1 displays a sample spectrum observed by MAESTRO and simulated by MODTRAN4 at a tangent height of 9.56 km in the troposphere.

The correlated-k option provides the most accuracy available in a band modeling approach and is computationally more efficient than a line-by-line simulation (*e.g.* Nowlan et al., 2007). MODTRAN is operated with 1 cm^{-1} spectral bins. Seventeen absorption coefficients per spectral bin are used. The difference in simulated optical depth between 17 and 33 k values was found to be trivial.

Except for water vapour, which is updated during the inversion and ozone, which is retrieved from MAESTRO v2.2 visible spectra beforehand using the approach described by McElroy et al. (2007), the appropriate MODTRAN4 model atmosphere is used. The relevant parameters include pressure and temperature. The MAESTRO-observed ozone profile is retrieved on the same tangent height grid and is only used in the water vapour retrieval range. Above the upper altitude of the water vapour retrieval, ozone and water vapour are also determined by the appropriate MODTRAN4 model atmosphere. The sensitivity to these forward model inputs is investigated in Section 2.1. In the simulations, the vertical grid above the retrieval range is 2 km up to 56 km, above which there

are atmospheric layers between 60 and 100 km in 10 km increments. Only for the first iteration of the retrieval, a simple linear regression is performed with the purpose of determining the noise level of the observations. This step is required to determine the convergence criterion for each vertical level of the retrieval. The gaseous differential absorption optical depth spectrum simulated for each tangent height ($DOD_{sim}(\lambda, TH)$) is fitted to the corresponding observed differential optical depth spectrum ($DOD_{obs}(\lambda, TH)$). The regression equation is:

$$DOD_{obs}(\lambda) = c_{sim} DOD_{sim}(\lambda) \quad (1)$$

where $c_{sim}(TH)$ is a unitless scaling coefficient. More importantly, the regression returns the relative standard error of the fitting coefficient ($\sigma_{sim}(TH)$), calculated as follows:

$$\sigma_{sim}(TH) = \left(\frac{\sum_{\lambda=1}^{N} [\delta(\lambda)]^2}{(N-k-1) \times c_{sim} \times \sum_{\lambda=1}^{N} [DOD_{sim}(\lambda)]^2} \right)^{0.5} \quad (2)$$

where $\delta(\lambda)$ is the residual of the regression at spectral pixel λ, N is the number of spectral pixels in the considered window, and k is the number of basis functions (=1). The TH dimension has been omitted from Eqs. (1) and (2) for the sake of simplicity. Because the retrieval uses wavelength-averaged optical depths, σ_{sim} is only expected to be proportional to the wavelength-averaged uncertainty. In the upper troposphere, σ_{sim} is frequently <1%, indicating the quality of the MAESTRO calibrated optical depth spectra. Given the >1% retrieval uncertainties due to spectroscopic parameters and other forward model inputs (see below), a single altitude-independent error scaling factor was empirically derived which, when multiplied by σ_{sim}, gives the convergence criterion for a given vertical layer. The error scaling factor was empirically determined by fitting optical depth spectra (with inherent noise) from a test ensemble of occultation events from August 2005. The error scaling factor was incremented in integer steps until the retrieval performed with expected success ratio (approaching 100%). The optimal error scaling factor was found to be 6. The convergence criterion is not allowed to be smaller than 3%, to account for uncertainty in the precision and accuracy in the line intensities. MODTRAN4 relies on the water vapour line intensities measured by Chevillard et al. (1989) which were included in the 1996 edition of HITRAN (Rothman et al., 1998).

After the convergence criterion profile is calculated, the simulated differential optical depth due to gaseous absorption (water vapour and ozone) is averaged over wavelength and is compared to the observed wavelength-averaged differential absorption optical depth. Thus, the retrieval condition can be written as:

$$1/N \sum_{\lambda=1}^{N} DOD_{obs}(\lambda, TH) = 1/N \sum_{\lambda=1}^{N} F(\boldsymbol{x}) \quad (3)$$

where $\boldsymbol{x}$ represents the vertical profiles of atmospheric parameters (water vapour, ozone, temperature, pressure), and F is the forward model which calculates $DOD_{sim}(\lambda, TH)$ based on the atmospheric conditions. Recall that water vapour is the only atmospheric parameter that is updated during each iteration of the inversion. If, at a given tangent height, the two spectrally averaged quantities agree within the convergence criterion, the altitude is flagged. If not, the next guess at the local H_2O(v) mixing ratio is obtained using Chahine's (1970) relaxation method. If the value of the convergence criterion at a given layer is >65%, the layer is not updated but rather the first guess profile is assumed for all retrieval iterations. This prevents the fitting of extremely noisy spectra which occasionally occurs, for example, due to radiation hits in the South Atlantic anomaly. The mixing ratio at all vertical levels are updated simultaneously. If all altitudes are flagged during the same iteration, the retrieval is complete. Otherwise, layer mixing ratios are updated, even if they are flagged, unless the difference between wavelength-averaged observed DODs and simulated DODs is less than the LDL. A vertical level of the retrieval can also be flagged if the mixing ratio falls below 1 pmol/mol. If the algorithm has not solved the inversion problem after 50 iterations, the retrieval is terminated and the profile is discarded.

After the inversion is complete, H_2O(v) mixing ratio precision profile is calculated by a numerical, perturbation analysis. The H_2O(v) mixing ratio is perturbed by 20 μmol/mol in a given layer and the relative change of the wavelength-averaged simulated differential optical depth at each tangent height ($\delta DOD_{sim}/DOD_{sim}$) is calculated and represents the perturbation sensitivity. For each tangent height, the ratio of the convergence criterion to the perturbation sensitivity is multiplied by the mixing ratio perturbation. The TH with the minimum value for this product provides the mixing ratio error for the perturbed altitude. The perturbation procedure is repeated for each retrieval altitude to determine the precision profile. We have verified the linearity of the calculated error bars by reducing the perturbation magnitude to 5 and 10 μmol/mol. A typical retrieval requires 55 s for the inversion and ~40 s for the precision calculation on a 3.19 GHz processor.

In this paper, we use the MAESTRO version 2.2 Level 1 data. Version 2.2 dramatically improves the calibration with respect to an instrument artifact arising from the detector.

As a quality-control measure, we compare simultaneously-observed MAESTRO and FTS ozone profiles (version 2.2) to identify TH shifts. The altitude registration of the FTS is accurate to better than ~350 m in the 12–20 km (Boone et al., 2005). MAESTRO profiles are shifted in the vertical direction to minimize the root-mean-square difference in the ozone number density profiles between the two instruments in the stratosphere. This gives a TH bias for each occultation event. Only occultation events for which the absolute value of the TH bias is <1.0 km are shown in Section 3.

2.1. Sensitivity studies and forward model errors

The vertical resolution of the retrieved profiles was determined numerically by a perturbation method. Observations were simulated for a randomly chosen MAESTRO measurement (sunset 10578) using the retrieved water vapour profile, perturbed by +100 μmol/mol in a given layer. The profile retrieved from this perturbed case was compared with the control case (*i.e.* no VMR perturbation). This perturbation and retrieval process was repeated for the lowest 13 layers of the retrieval. The following observations resulted.

(1) There is no change in the retrieved profile between the perturbed and control case above the perturbed layer.
(2) The retrieved perturbation at the perturbed layer approaches 100% of the true perturbation (see Fig. 2). At lower (perturbation) altitudes, the retrieved perturbation may be not be quite 100% of the true perturbation (*e.g.* 85%).
(3) The retrieved perturbation below the perturbed layer is small (a few percent of the magnitude of the true perturbation in the perturbed layer) and is of the same sign as the perturbation. Its magnitude tends to be smaller at higher (perturbation) altitudes. Two layers below the perturbed layer, the retrieved perturbation is of the same magnitude as the one retrieved in the immediately overlying layer (and immediately below the perturbed layer) but of opposite sign. This is a retrieval oscillation and is a characteristic of direct (unregularized) retrieval. For layers below this, the retrieved perturbation dampens monotonically to 0% but there is a minor (1%), yet repeatable response even eight layers below the perturbed one. Overall, the retrieval overresponds slightly, indicating a positive bias on the order of a few percent to the partial column amount of water vapour.

The first two findings are expected for a retrieval without regularization for occultation geometry. The apparent spreading of the response at the lowest altitudes (not shown, but noted above) to altitudes below the perturbation altitude may be a result of a finer vertical grid there, which arises in the measurements due to the shifting upward of the radiometric centre of the sun within the FOV because of the strong vertical gradient in extinction in the troposphere. It is concluded, according to this numerical perturbation analysis, that the vertical resolution of the retrieved profiles approaches the limit of the step size of the altitude grid (Roscoe and Hill, 2002), which is 1 km or less.

In the top retrieval layer, there is sensitivity to the assumed water vapour profile above the retrieval range. This sensitivity was tested by changing the guessed (tropical) water vapour profile to a mid-latitude summer profile. Differences of 5% were observed in the top retrieval layer when retrieved with this profile. The second layer from the top shows a minor error (1%) of the opposite sign as the retrieval differences are expected to oscillate and dampen with decreasing height, especially since the water vapour optical depth grows rapidly with decreasing tangent height. Underlying layers are not affected significantly by the assumed profile above the retrieval range.

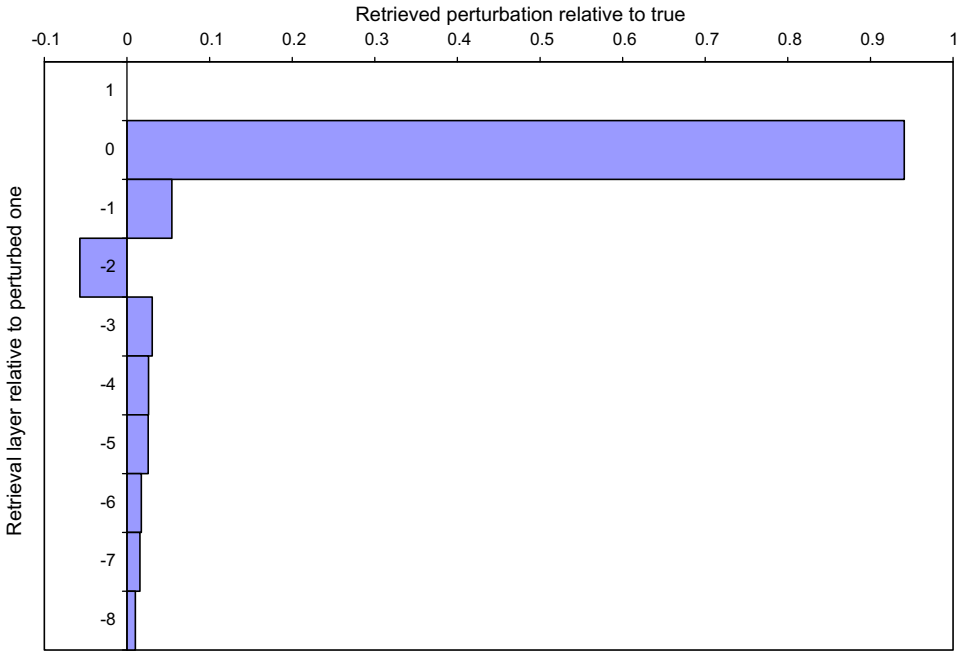

Fig. 2. Response of retrieval to perturbation in a single layer (namely layer '0'). The lack of response at overlying and underlying layers indicates that the retrieval approaches the limit of the vertical sampling.

The sensitivity of the retrieval to aerosols was investigated by comparing water vapour volume mixing ratios (VMRs) retrieved from simulated observations using the spring/summer MODTRAN4 aerosol profile with those retrieved using the fall/winter profile. The largest relative difference was at the top of the retrieved profile (25 km) whereas the largest absolute difference was at the bottom of the retrieved profile (5 km). At a tangent height of 25 km, the seasonal change in aerosol leads to less than a 0.002 difference in aerosol optical depth, and results in ~3% differences in the retrieved water vapour mixing ratio. The differences in retrieved $H_2O(v)$ appear to be completely random and stem from the imperfect removal of the baseline optical depth due to aerosol extinction by assuming a linear function with respect to wavelength. At a tangent height of 5 km, the seasonal variation in aerosol abundance and extinction leads to a change in aerosol optical depth of 0.65. Yet, the retrieval error is only 1.25 μmol/mol (or 0.08%). This indicates the major advantage of full spectral measurements over the use of discrete wavelengths (*e.g.* POAM III, see above) for the remote sounding of water vapour in the presence of high concentrations of tropospheric aerosol.

We have also tested the sensitivity to the pre-measured ozone profile. MAESTRO ozone was recently validated (Dupuy et al., 2009) and found to generally agree with various coincident satellite-borne, airborne, balloon-borne and ground-based instruments within ±5% for sunrise and sunset between 18 and 40 km. The comparison with POAM III typically showed differences of ±4% between 12 and 40 km (Dupuy et al., 2009). With ozone measured to this accuracy, resulting biases in water vapour in this height range are not significant. Below 12 km, 10% biases in O_3 lead to ~0.1% biases in water vapour, because the absorption signal from water vapour is dominant, and ozone interference is negligible.

The sensitivity to errors in the assumed temperature and pressure profiles were tested independently by using a MODTRAN4 mid-latitude summer profile instead of a tropical one. For temperature, this perturbation amounts to a ~2 K cooling through the upper troposphere. The resulting change in retrieved water vapour in the troposphere is typically ~0.6%. In the lower stratosphere (14–25 km), the mid-latitude summer temperature profile is, on average, 12 K warmer than the tropical one. The resulting mean water vapour bias is ~0.1 μmol/mol, indicating that temperature is a minor source of model-input-parameter error (~2%) in the lower stratosphere as well. The mid-latitude summer (MLS) pressure is 5 mb lower than the tropical one through the upper troposphere. This results in a retrieval error of 2%. In the lower stratosphere, retrieval biases are insignificant for a typical pressure bias of ~2 mb.

3. Results

Fig. 3 shows a sample comparison of collocated water vapour profiles simultaneously observed by MAESTRO, FTS and MLS in the tropical troposphere and lower stratosphere. FTS water vapour has been validated (Car-

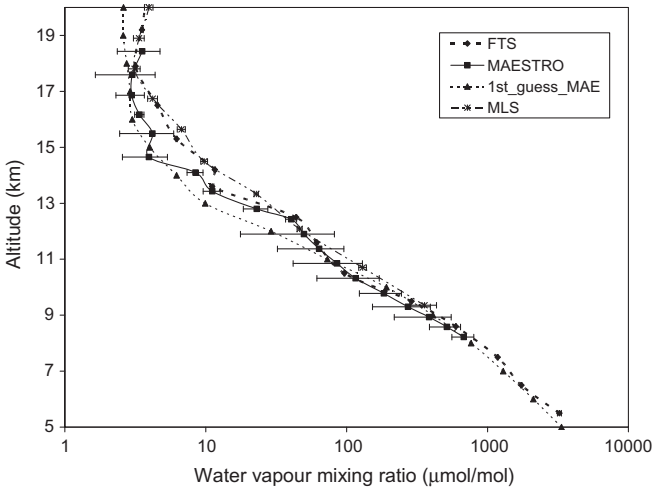

Fig. 3. Sample profile comparison for sunset 8922 just south of the island of Java, Indonesia (9.6°S, 111°E) on 9 April 2005. Note the logarithmic scale. The 'first guess' tropical profile ('1st_guess_MAE') is also shown. The uncertainty shown for MAESTRO at altitudes above 13 km is the standard deviation of the concentration in that layer and the layers immediately above and below, after removal of the quadratic trend versus altitude in this range. Aura-MLS observed at 10.4°S, 109.3°E about 17 h earlier. The MLS altitudes were obtained by linear interpolation using the relationship between altitude and the natural logarithm of the pressure from FTS.

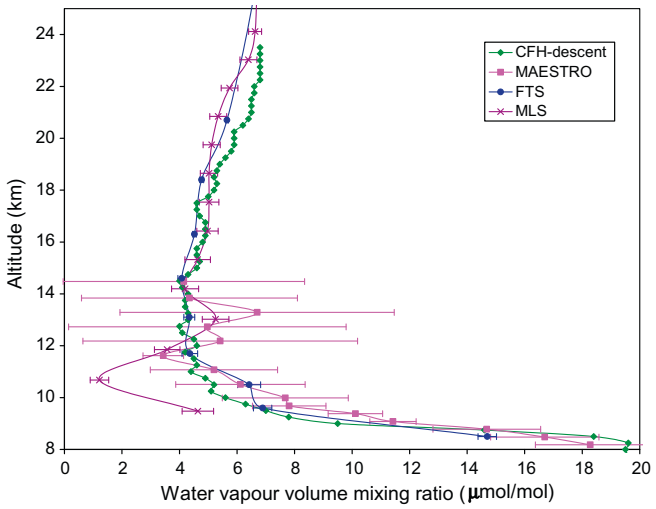

Fig. 4. Validation of profiles observed by MAESTRO, FTS during sunrise 7933 over Sodankylä, Finland on 1 February 2005 at 07:40 UT with the coincident in situ profile measured by the CFH at 16:40 UT. The distance between the ACE measurement location (65.6°N, 21.0°E) and the balloon was 310 km. The MAESTRO profile shown is a three-point running mean (to reduce noise) and was shifted downward by 0.73 km, based on the altitude shift obtained from a comparison of MAESTRO and FTS ozone profiles (see Section 2). The uncertainty shown for MAESTRO is the standard deviation of the concentration in that layer and the layers immediately above and below after removal of the quadratic trend versus altitude. The Aura-MLS (nearest) observation at 68.9°N, 24.0°E occurred in the early afternoon of the same day.

leer et al., 2008) and has been used in the validation of Aura-MLS water vapour (Lambert et al., 2007). For the example shown in Fig. 3, the thermal tropopause is at 16.5 km according to the FTS data. The change in the water vapour gradient at 12.5 km corresponds to the boundary between the free troposphere and the tropical tropopause layer. Convective transport of water vapour is generally limited to altitudes below ~12 km and thus, above this altitude, there is a strong gradient to significantly lower VMRs. The profiles for the three instruments are in agreement, particularly below 14 km, where the increase in number density of water vapour facilitates the MAESTRO retrieval. Aura-MLS sampled on either side of the location of the ACE observations. The more correlated of the two MLS profiles (version 2.2) is illustrated in Fig. 3.

For a single profile validation of water vapour in the UT/LS, the current standard appears to be the cryogenic frost point hygrometer (CFH) (Vömel et al., 2007). Only one frost point hygrometer profile coincident with a MAESTRO profile was found after searching for coincidences on a given calendar day within 4° of latitude and 12° of longitude in the period 2004–2006 (Fig. 4). This measurement coincidence occurred in polar winter, providing much drier conditions below 14 km than the case in Fig. 3. This leads to a noisier MAESTRO profile although the magni-

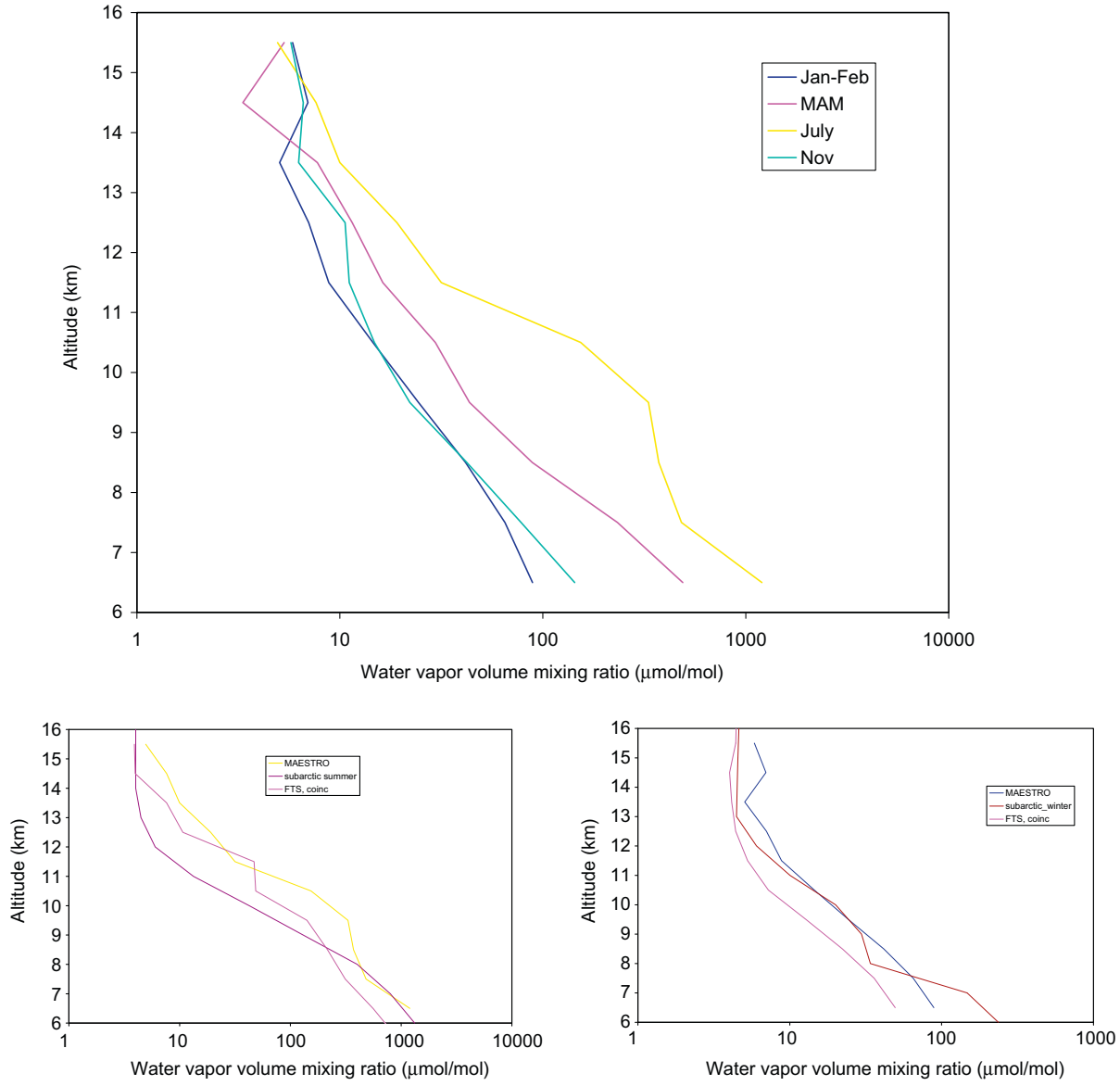

Fig. 5. (a: top) MAESTRO water vapour median VMR profiles in the UT/LS as a function of season for 2006 in the 60 to 70°N band. The sample size is small for July, March–May (MAM) below 9 and 8 km, respectively, due to thick clouds. In the September–November period, the sample size is small (N = 14) at all altitudes as this latitude is only sampled in November due to gaps in data collection. (b: bottom left) Comparison of high-latitude summer water vapour VMR profiles as observed by MAESTRO and FTS in July 2006 (60 to 70°N) and the standard model atmosphere for July 60°N ("subarctic summer"). (c: bottom right) same as (b), except for January–February 2006. The standard model atmosphere is for January 60°N ("subarctic winter"). In Figs. 5b–c, the same subset of profiles used for MAESTRO was also used for FTS.

tude and gradient in water vapour mixing ratio in the upper troposphere are well captured given the agreement with FTS and CFH.

The seasonal cycle of water vapour in the boreal high latitude (60–70°N) upper troposphere is shown in Fig. 5. This latitude band was selected because ACE samples it more than any other band. As noted in the caption, thick clouds limit the retrieval range, particularly in summer, when deep convection reaches higher altitudes and latitudes. At 15.5 km, the profiles representing the four seasons are within <1 μmol/mol of each other, indicating that the weak seasonal cycle of water vapour at this latitude in the lower stratosphere. The VMR is ~5 μmol/mol. At 9.5 km, there is more than an order of magnitude more water vapour in July than in January–February. This large factor is largely attributable to advection from low latitudes and convection (including that occurring at lower latitudes) and depends less on seasonal differences in saturation vapour pressure (which would only lead to a factor of ~2.7, assuming an 8 K change from 217 to 225 K). For July (Fig. 5b), above 8.5 km, both FTS and MAESTRO show higher water vapour VMRs than the sub-arctic summer atmosphere. The low bias of the sub-arctic summer model atmosphere is significant only for FTS data at 11.5 km. The bias between the two ACE instruments is not significant at any altitude in either summer or winter. However, there is a significant positive bias in water vapour VMR between the sub-arctic winter model atmosphere at 6.5 km and MAESTRO (January–February, 60–70°N) that is confirmed by FTS. The latter instrument, with better precision than MAESTRO at low VMRs, indicates that the positive bias extends to the following altitude bins: 7.5, 9.5–11.5, and 14.5 km.

In the lower troposphere, water vapour volume mixing ratios are expected to be larger in the southern hemisphere (SH) than the northern hemisphere (NH) due to differences in oceanic evaporation (Price, 2000), stemming from the greater fractional area covered by oceans in the SH. On the other hand, deep convection is more intense over land, particularly in summertime, and is thus more prevalent in the NH. Deep convection significantly raises the concentration of water vapour in the summertime high-latitude upper troposphere (as seen in Fig. 5). MAESTRO observations are consistent with the current understanding of the vertical distribution of the interhemispheric ratio of water vapour in the middle and upper troposphere (Fig. 6). At 5.5 km, there is 40% more water vapour in the SH than the NH. At 6.5 km, the contribution by deep convection begins to dominate the contribution of oceanic evaporation in determining the local water vapour concentration. At 10.5 km, the NH/SH water vapour ratio reaches a maximum of 2.35, with deep convection largely governing the abundance of water vapour. At high latitudes, higher altitudes are above the tropopause, and not influenced by convection so the interhemispheric ratio approaches one. FTS shows a similar tendency with altitude except at 5.5 km and a positive bias in the interhemispheric ratio. FTS has been

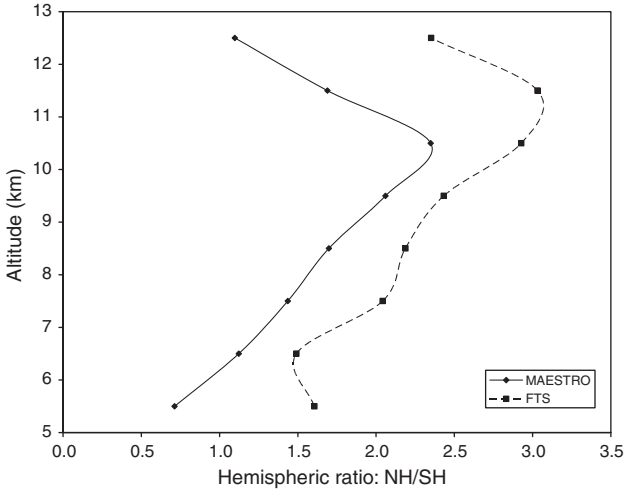

Fig. 6. Vertical profile of interhemispheric ratio of water vapour observed by MAESTRO and FTS in summer (June–August in northern hemisphere, December–February in southern hemisphere). Hemispheric median profiles are calculated using retrieved data from December 2004 to August 2006.

thoroughly validated only down to 10 km, where it consistently shows positive biases ($\geqslant$20%) versus all correlative satellite instruments (SAGE II, POAM III, MIPAS, and HALOE).

4. Concluding remarks

The MAESTRO water vapour data record currently extends from February 2004 to January 2009, a period of almost 5 years. The instrument continues to function nominally at the present time.

The accuracy of the middle tropospheric H_2O(v) profile by MAESTRO may be dominated by the accuracy of absorption line intensities, given the high precision of the measurement in this region. As the algorithm develops further, another minor source of error which can be reduced involves using the pressure profile contained in FTS data rather than pressures from a model with coarse latitudinal and temporal binning.

A new version (3.0) of MAESTRO Level 1 data will soon be available for the entire data record. This new data promises improved tangent height determination relative to version 2.2 and may be used to statistically analyze whether significant differences between FTS and MAESTRO remain.

Averaged MAESTRO data may have a low bias resulting from its inability to measure through optically thick cloud. This bias will be common to other satellite instruments measuring in the visible and infrared spectral regions.

As illustrated above, MAESTRO is capable of accurately measuring fine structure in the vertical profile of water vapour, particularly in the middle and upper troposphere. This capability and the retrieval range from the lower stratosphere to 5 km make this a unique data prod-

uct among those provided by the current generation of Earth-observing satellite instruments.

References

Berk, A., Anderson, G.P., Acharya, P.K., Chetwynd, J.H., Bernstein, L.S., Shettle, E.P., Matthew, M.W., Adler-Golden, S.M. MODTRAN4 User's Manual: Software Manual. Air Force Res. Lab., Space Vehicles Dir., Air Force Mater, Command, Hanscom Air Force Base, Mass, 1999.

Bernath, P. Spectra of Atoms and Molecules. Oxford University Press, Oxford, 1995.

Boone, C.D., Nassar, R., Walker, K.A., Rochon, Y., McLeod, S.D., Rinsland, C.P., Bernath, P.F. Retrievals for the Atmospheric Chemistry Experiment Fourier-transform spectrometer. Appl. Opt. 44, 7218–7231, 2005.

Carleer, M.R. et al. Validation of water vapour profiles from the Atmospheric Chemistry Experiment (ACE). Atmos. Chem. Phys. Discuss. 8, 4499–4559, 2008.

Chahine, M.T. Inverse problems in radiative transfer: determination of atmospheric parameters. J. Atmos. Sci. 27, 960–967, 1970.

Chevillard, J.-P., Mandin, J.-Y., Flaud, J.-M., Camy-Peyret, C. $H_2{}^{16}O$: line positions and intensities between 9500 and 11500 cm^{-1}. The interacting vibrational states (0 4 1), (2 2 0), (1 2 1), (0 2 2), (3 0 0), (2 0 1), (1 0 2), and (0 0 3). Can. J. Phys. 67, 1065–1084, 1989.

Dupuy, E. et al. Validation of ozone measurements from the Atmospheric Chemistry Experiment (ACE). Atmos. Chem. Phys. 9, 287–343, 2009.

El Helou, Z., Churassy, S., Wannous, G., Bacis, R., Boursey, E. Absolute cross sections of ozone at atmospheric temperatures for the Wulf and Chappuis bands. J. Chem. Phys. 122, 244311-1–244311-9, 2005.

Gettelman, A. et al. Validation of Aqua satellite data in the upper troposphere and lower stratosphere with in situ aircraft instruments. Geophys. Res. Lett. 31, L22107, doi:10.1029/2004GL020730, 2004.

Kirk-Davidoff, D.B., Hintsa, E.J., Anderson, J.G., Keith, D.W. The effect of climate change on ozone depletion through changes in stratospheric water vapour. Nature 402, 399–401, 1999.

Lambert, A. et al. Validation of the Aura Microwave Limb Sounder middle atmosphere water vapor and nitrous oxide measurements. J. Geophys. Res. 112, D24S36, doi:10.1029/2007JD008724, 2007.

Lumpe, J., Bevilacqua, R.M., Hoppel, K.W., Randall, C.E. POAM III retrieval algorithm and error analysis. J. Geophys. Res. 107 (D21), 4575, doi:10.1029/2002JD002173, 2002.

McElroy, C.T. et al. The ACE-MAESTRO instrument on SCISAT: description, performance, and preliminary results. Appl. Opt. 46, 4341–4356, 2007.

Milz, M. et al. Water vapor distributions measured with the Michelson Interferometer for Passive Atmospheric Sounding on board Envisat (MIPAS/Envisat). J. Geophys. Res. 110, D24307, doi:10.1029/2005JD005973, 2005.

Nassar, R., Bernath, P.F., Boone, C.D., Manney, G.L., McLeod, S.D., Rinsland, C.P., Skelton, R., Walker, K.A. Stratospheric abundances of water and methane based on ACE-FTS measurements. Geophys. Res. Lett. 32, L15S04, doi:10.1029/2005GL022383, 2005.

Nowlan, C.R., McElroy, C.T., Drummond, J.R. Measurements of the O_2 *A*- and *B*-bands for determining temperature and pressure profiles from ACE-MAESTRO: forward model and retrieval algorithm. J. Quant. Spectrosc. Rad. Transfer 108, 371–388, 2007.

Price, C. Evidence for a link between global lightning activity and upper tropospheric water vapour. Nature 406, 290–293, 2000.

Roscoe, H.K., Hill, J.G.T. Vertical resolution of oversampled limb-sounding measurements from satellites and aircraft. J. Quant. Spectrosc. Rad. Transfer 72, 237–248, 2002.

Rothman, L.S. et al. The HITRAN molecular spectroscopic database and HAWKS (HITRAN atmospheric workstation): 1996 edition. J. Quant. Spectrosc. Rad. Transfer 60, 665–710, 1998.

Su, H., Read, W.G., Jiang, J.H., Waters, J.W., Wu, D.L., Fetzer, E.J. Enhanced positive water vapor feedback associated with tropical deep convection: new evidence from Aura MLS. Geophys. Res. Lett. 33, L05709, doi:10.1029/2005GL025505, 2006.

Taha, G., Thomason, L.W., Burton, S.P. Comparison of Stratospheric Aerosol and Gas Experiment (SAGE) II version 6.2 water vapor with balloon-borne and space-based instruments. J. Geophys. Res. 109, D18313, doi:10.1029/2004JD004859, 2004.

Vömel, H., David, D.E., Smith, K. Accuracy of tropospheric and stratospheric water vapor measurements by the cryogenic frost point hygrometer: Instrument details and observations. J. Geophys. Res. 112, D08305, doi:10.1029/2006JD007224, 2007.